



Williams meets von Karman: Mode coupling and nonlinearity in the fracture of thin plates

CHUNG-YUEN HUI, ALAN T. ZEHNDER and YOGESH K. POTDAR

Department of Theoretical and Applied Mechanics, Cornell University, 313-4, Kimball Hall, Ithaca, NY 14853-1503 USA; e-mail: ch45@cornell.edu

Received 28 January 1998; accepted in revised form 11 August 1998

Abstract. The stress field near the tip of a crack in a plate subjected to membrane and bending loads and undergoing large deflections, is investigated by performing an asymptotic analysis in the context of von Karman plate theory. It is demonstrated that the character of the near tip fields is identical to those of the linear plate theory. However, the determination of the crack tip stress intensity factors requires the solution of a large deflection, and hence nonlinear, problem due to the coupling of the membrane and bending modes. This effect is illustrated through the solution of three fracture problems involving plates of simple geometries loaded by pressure, tension and shearing. In two of these problems, the energy release rate is obtained exactly. Nonlinear finite element computations are performed to obtain the stress intensity factors and energy release rate associated with tension, bending and shearing. These results are compared to the theoretical results for energy release rate and stress intensity factors.

Key words: Stress intensity factor, plate theory, energy release rate, finite element method, large deflection.

1. Introduction

Recent interest in aircraft structural integrity has led to renewed research in the problem of fracture of cracked, elastic thin plates (Williams, 1962; Sih et al. 1962; Knowles and Wang, 1960; Wang, 1970; Delale and Erdogan, 1979; Murthy et al. 1981; Boduroglu and Erdogan, 1983; Simmonds and Duva, 1981; Young and Sun, 1993ab; Alwar and Thiagarajan, 1989; Hui and Zehnder, 1993, 1994; Viz et al. 1995ab; Viz and Zehnder, 1994; Viz, 1996) under combined bending, twisting and in-plane loading conditions. Research in this field, however, is not new; and has its origins in William's 1961 paper on crack tip fields in the small deflection, Kirchhoff plate theory (Kirchhoff, 1950). Theories of fracture based on those results had considerable success, but, in principle, are limited in application to structures in which the deflections are small. In practice, this limitation to small deflections has stopped no one. It does, however, lead to the question: Do the Kirchhoff theory fields still describe the crack tip stresses when large deflections occur? This question is answered here by performing an asymptotic analysis in the context of the large deflection plate theory developed by von Karman (1910). The assumption of small deflections used in the existing analyses of crack tip fields enables the membrane stresses due to in-plane loading to be decoupled from the stresses due to bending, twisting, and shearing loading. In Kirchhoff theory, the crack tip stress and displacement fields, with respect to a polar coordinate system (r, θ) located at the mid-plane

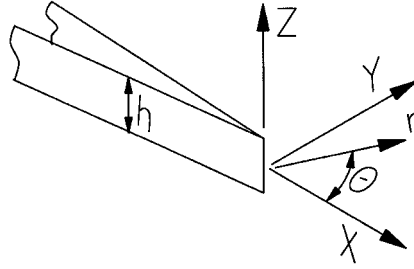


Figure 1. Geometry illustrating the crack tip coordinate system.

of the plate, $z = 0$, (see Figure 1), have the form (as $r \rightarrow 0$) (Williams, 1961; Sih et al. 1962; Murakami, 1987)

$$\boldsymbol{\sigma} = \frac{K_I}{\sqrt{2\pi r}} \mathbf{f}^I(\theta) + \frac{K_{II}}{\sqrt{2\pi r}} \mathbf{f}^{II}(\theta) + \frac{k_1}{\sqrt{2r}} \frac{2z}{h} \mathbf{k}^I(\theta) + \frac{k_2}{\sqrt{2r}} \frac{2z}{h} \mathbf{k}^{II}(\theta), \quad (1a)$$

$$\mathbf{u} = \frac{(1+\nu)K_I\sqrt{r}}{E\sqrt{2\pi}} \hat{\mathbf{u}}^I(\theta) + \frac{(1+\nu)K_{II}\sqrt{r}}{E\sqrt{2\pi}} \hat{\mathbf{u}}^{II}(\theta), \quad (1b)$$

$$w = \frac{k_1(2r)^{3/2}}{2Eh} \hat{w}^I(\theta) + \frac{k_2(2r)^{3/2}}{2Eh} \hat{w}^{II}(\theta), \quad (1c)$$

where E , ν are the Young's modulus and the Poisson's ratio respectively and h is the plate thickness. The in-plane stress tensor and displacement vector are denoted by $\boldsymbol{\sigma}$ and \mathbf{u} respectively. The out of plane plate deflection is denoted by w . All tensor and vector functions are denoted by boldface letters. The classical Mode I and Mode II stress intensity factors are denoted by K_I , K_{II} respectively. The Kirchhoff stress intensity factors are denoted by k_1 , k_2 which represent, respectively, a symmetric bending mode and an antisymmetric twisting/transverse shearing mode. These modes are illustrated schematically in Figure 2. The dimensionless functions $\mathbf{f}^I(\theta)$, $\mathbf{f}^{II}(\theta)$, $\mathbf{k}^I(\theta)$, $\mathbf{k}^{II}(\theta)$ and $\hat{\mathbf{u}}^I(\theta)$, $\hat{\mathbf{u}}^{II}(\theta)$, $\hat{w}^I(\theta)$, $\hat{w}^{II}(\theta)$ describe the angular variations of the crack tip fields and can be found in (Williams, 1961; Sih et al. 1962; Hui and Zehnder, 1993; Viz, 1996). The bending and membrane modes are decoupled since, for small deflections, K_I , K_{II} and k_1 , k_2 can be obtained independently by solving two uncoupled, linear elastic crack problems. A consequence is that these stress intensity factors are directly proportional to the external loading parameters.

The crack tip fields resulting from Kirchhoff plate theory differ from the usual three dimensional elasticity solution. Indeed, the transverse shear stresses (σ_{xz} , σ_{yz}) vary asymptotically as $r^{-3/2}$ instead of $r^{-1/2}$ as $r \rightarrow 0$. Furthermore, the angular distributions of the Kirchhoff theory stress field differ from the linear elastic planar fracture mechanics results. For these reasons, the asymptotic stress field has also been calculated by many researchers using Reissner plate theory (Knowless and Wang, 1960; Wang, 1970; Dalale and Erdogan, 1979; Murthy et al. 1981). The asymptotic crack tip fields in Reissner plate theory all vary as $r^{-1/2}$ as $r \rightarrow 0$. Furthermore, they have identical angular distributions as those from planar elasticity. However, the use of Kirchhoff plate theory is justified by an asymptotic argument similar to that of small scale yielding in elastic-plastic fracture mechanics. Specifically, the Kirchhoff crack tip fields may be interpreted as the far field boundary conditions for the near tip Reissner crack tip fields. Indeed, Hui and Zehnder (1993) as well as Young and Sun (1993a) have shown independently

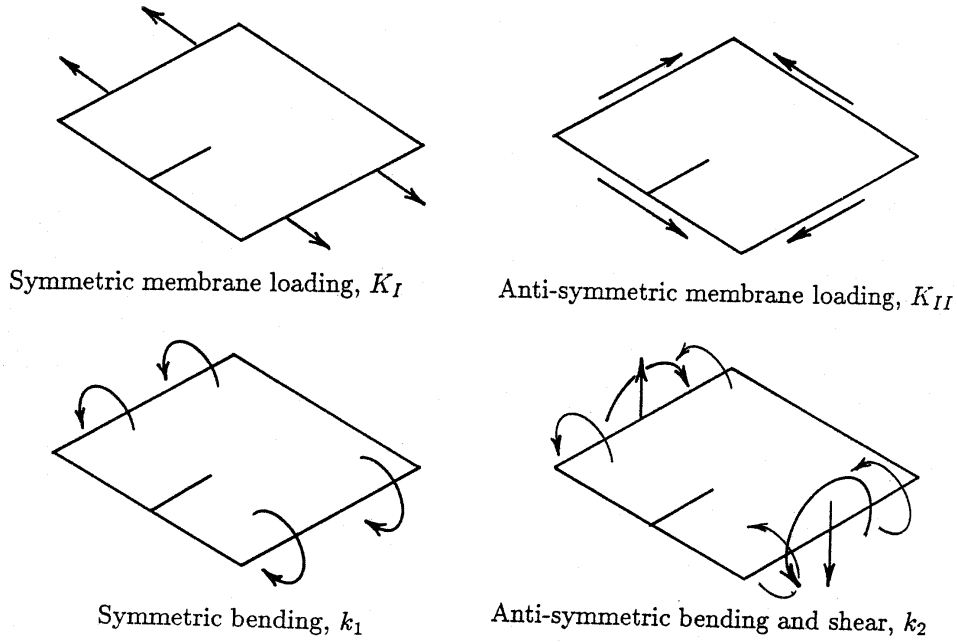


Figure 2. Fracture modes for a Kirchhoff cracked plate and their associated stress intensity factors, K_I, K_{II} represent the plane stress modes and k_1, k_2 represent the Kirchhoff plate theory modes.

that there is a unique relation between the Kirchhoff stress intensity factors and the Reissner stress intensity factors in the limit of very thin plates. This unique relation is universal in the sense that it is independent of the specimen geometry and loading configurations.

For self-similar crack growth, the energy release rate G is related to the stress intensity factors by (Hui and Zehnder, 1993)

$$\begin{aligned}
 G &= \frac{K_I^2}{E} + \frac{K_{II}^2}{E} + \frac{\pi(1+\nu)k_1^2}{3(3+\nu)E} + \frac{\pi(1+\nu)k_2^2}{3(3+\nu)E}, \\
 &= G_I + G_{II} + g_1 + g_2,
 \end{aligned}
 \tag{2}$$

where the G_I, G_{II}, g_1, g_2 are the energy release rate components associated with the different fracture modes. It is important to note that since (2) follows from (1a–c) through a virtual crack extension argument, it is valid as long as the crack tip fields have the form given by (1); even if K_I, K_{II} and k_1, k_2 are interdependent and are nonlinear functions of the external loads.

A serious limitation of the linearized Kirchhoff theory is that it is only valid when the plate deflection is much smaller than the plate thickness. For cracks in aircraft structures, and in the experiments performed by Viz et al. (1995b), the plate deflections can be many times the plate thickness. In this regime, the coupling of the membrane and bending stresses is extremely important and the simple approximation of independently computing (K_I, K_{II}) from the membrane loads and (k_1, k_2) from the bending loads leads to large errors, as we will demonstrate below. Furthermore, it is not clear whether the near tip fields are still given by (1a–1c) if a large deflection plate theory is used in the analysis.

The goal of this work is to characterize the crack tip fields and to investigate the nonlinear coupling of the membrane and bending modes of fracture using von Karman’s nonlinear, large deflection theory of elastic plates. This theory allows for the plate deflection to be on

the order of the plate thickness (Von Karman, 1910; Fung, 1965). We first show that the asymptotic stress field given by (1a–1c), and hence the energy release rate given by (2) are still valid for a von Karman plate except that now (K_I, K_{II}) and (k_1, k_2) are generally not independent of each other, but are nonlinear functions of the external loads. The coupling between membrane and bending/shearing modes will be illustrated by three crack problems involving thin, cracked elastic plates of simple geometries. These problems will be studied analytically and numerically. In two of these problems, the energy release rate can be obtained in closed form. In the third problem, approximate results are obtained.

2. Crack tip fields in a Von Karman plate

2.1. SUMMARY OF VON KARMAN PLATE EQUATIONS

The governing equations of a von Karman plate in the absence of in plane body forces, expressed in terms of the plate deflection, $w(x, y)$, and the Airy stress function, $F(x, y)$ are (Fung, 1965)

$$\nabla^4 w = D^{-1}[p + B(F, w)], \quad (3a)$$

$$\nabla^4 F = EhA(w), \quad (3b)$$

where $D = Eh^3/12(1 - \nu^2)$, p is the pressure acting on the plate, and B and A are nonlinear differential operators defined by

$$B(F, w) \equiv F_{,yy}w_{,xx} + 2F_{,xy}w_{,xy} + F_{,xx}w_{,yy}, \quad (3c)$$

$$A(w) \equiv (w_{,xy})^2 + w_{,xx}w_{,yy}. \quad (3d)$$

The comma denotes partial derivative, e.g. $w_{,xy} = \partial^2 w / \partial x \partial y$.

The membrane forces (force/unit length) \mathbf{N} are related to F by

$$N_{xx} = F_{,yy}, N_{yy} = F_{,xx}, N_{xy} = -F_{,xy}. \quad (4a)$$

The membrane forces and the bending and twisting moments \mathbf{M} are related to the displacements by

$$\begin{aligned} N_{xx} &= \frac{Eh}{1 - \nu^2} \left[u_{x,x} + \nu u_{y,y} + \frac{1}{2}(w_{,x})^2 + \frac{\nu(w_{,y})^2}{2} \right], \\ N_{yy} &= \frac{Eh}{1 - \nu^2} \left[u_{y,y} + \nu u_{x,x} + \frac{1}{2}(w_{,y})^2 + \frac{\nu(w_{,x})^2}{2} \right], \\ N_{xy} &= \frac{Eh}{2(1 + \nu)} (u_{x,y} + u_{y,x} + w_{,y} w_{,x}), \\ M_{xx} &= -D(w_{,xx} + \nu w_{,yy}), \quad M_{yy} = -D(w_{,yy} + \nu w_{,xx}), \\ M_{xy} &= -D(1 - \nu)w_{,xy}. \end{aligned} \quad (4b)$$

2.2. ASYMPTOTIC ANALYSIS

Since we are interested in crack tip fields, the crack can be considered as semi-infinite. Assume that the crack lies on the negative x axis with its tip at the origin. The traction free boundary conditions consistent with plate theory are

$$N_{yy}(r, \theta = \pm\pi) = N_{xy}(r, \theta = \pm\pi) = 0, \quad (5a)$$

$$M_{yy}(r, \theta = \pm\pi) = [Q_y(r, \theta = \pm\pi) + M_{xy,x}(r, \theta = \pm\pi)] = 0, \quad (5b)$$

where Q_y is the y component of the transverse shear resultant \mathbf{Q} which is given by

$$Q_x = -D\nabla^2 w_{,x} + N_{xx}w_{,x} + N_{xy}w_{,y}, \quad (5c)$$

$$Q_y = -D\nabla^2 w_{,y} + N_{xy}w_{,x} + N_{yy}w_{,y}.$$

Note that the nonlinear terms appear both in the differential equations, i.e., $B(F, w)$, $A(w)$, as well as in the boundary conditions. The linear theory neglects these nonlinear terms resulting in the uncoupling of the differential equations and of the boundary conditions. Specifically, the asymptotic results of the linear theory (1a–c) satisfy equations (3,4,5) with all the nonlinear terms removed.

We now show that the asymptotic results given by (1a–c) are still valid for a von Karman plate. The simplest way to see this is to note that the nonlinear terms, $B(F, w)$ and $A(w)$, in the differential equations, as well as in the boundary conditions vanish in comparison to the linear terms as $r \rightarrow 0$. In the language of asymptotic analysis, these terms are subdominant. Indeed, using (1a–1c), one can easily verify that

$$B(F, w) = O(r^{-1}), \quad A(F, w) = O(r^{-1}), \quad r \rightarrow 0, \quad (6)$$

whereas the asymptotic behavior of the LHS of (3a–b) is

$$\nabla^4 w = O(r^{-5/2}), \quad \nabla^4 F = O(r^{-5/2}), \quad r \rightarrow 0. \quad (7)$$

Likewise, in the boundary conditions, e.g. $N_{yy}(r, \theta = \pm\pi) = 0$, we have, as $r \rightarrow 0$

$$\begin{aligned} N_{yy} &= \frac{Eh}{1-\nu^2} \left[u_{y,y} + \nu u_{x,x} + \frac{(w_{,y})^2}{2} + \frac{\nu(w_{,x})^2}{2} \right] \\ &\approx \frac{Eh}{1-\nu^2} [u_{y,y} + \nu u_{x,x}], \end{aligned}$$

since the term

$$\frac{(w_{,y})^2}{2} + \frac{\nu(w_{,x})^2}{2} = O(r), \quad r \rightarrow 0,$$

whereas the term

$$u_{y,y} + \nu u_{x,x} = O(r^{-1/2}), \quad r \rightarrow 0,$$

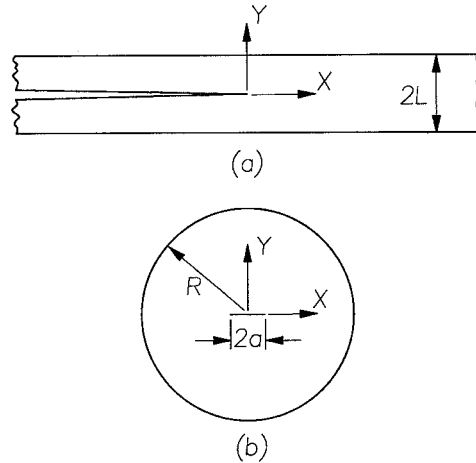


Figure 3. Example problems analyzed: (a) Infinite strip with a semi-infinite crack. Top and bottom edges clamped. Plate loaded either by stretching combined with uniform pressure, or by out of plane shearing. (b) Clamped circular plate of radius R , under uniform pressure, containing a small crack of length $2a$.

so that the term $[(w_{,y})^2 + \nu(w_{,x})^2]/2$ becomes negligible with respect to $u_{y,y} + \nu u_{x,x}$. In other words, the first order asymptotic behavior of the stress and deformation fields is completely determined by the linear terms of the governing equations and the boundary conditions. Therefore, the asymptotic results of (1a–1c) still apply for the case of a von Karman plate. This, however, does not imply that the stress intensity factors can be determined by the linear theory, since they can only be determined by solving the full set of nonlinear, coupled equations.

Of course, one can start with the formal approach assuming F and w must have the form

$$F = r^\lambda \hat{F}(\theta), \quad w = r^{\lambda+1} \hat{w}(\theta)$$

and proceed with the asymptotic method of William's. As before, this procedure will show that the nonlinear terms are subdominant so that the results will be identical to that of (1a–c).

3. Nonlinear solutions illustrating mode coupling: three examples

In most real-world problems involving cracked plates or shells the out of plane deflections are relatively large. Depending on the boundary conditions these large deflections can result in membrane stresses as well as the bending stresses associated with the linear plate theories. As seen in equation (3), when the membrane stresses must be included there results a set of nonlinear, coupled equations. For complex geometries these equations must be solved numerically using geometrically nonlinear finite element methods. There are however a number of simple geometries for which analytical solutions can be obtained. These solutions demonstrate the coupling between the membrane and bending fracture modes, show how the different stress intensity factor and energy release rate components scale with the applied loads or displacements, and provide nonlinear benchmark solutions against which numerical analysts can test their numerical procedures.

The three examples given in this paper are illustrated in Figure 3. The first two are problems involving an infinite strip with an semi-infinite crack. The edges of the strip, located at $y =$

$\pm L$ are clamped and the strip is loaded either by a uniform pressure combined with in-plane stretching or by out-of-plane shearing. The third problem is for a small crack in a clamped, circular plate under uniform pressure. The infinite strip problems are solved exactly for G using an energy approach. The circular plate solution is approximate, but quite accurate for small cracks. It is a stress based method that uses a simple interpolation of the membrane stress and bending moment to determine K_I and k_I . Finite element solutions of all three problems are given since in some cases the individual components of energy release rate, and hence the stress intensity factors cannot be determined from the analytical results, although the total energy release rate may be known exactly.

3.1. FINITE ELEMENT PROCEDURES

The energy release rates defined in (2) were computed using the modified crack closure integral (MCCI) (Viz et al. 1995a) method in conjunction with geometrically nonlinear finite element analyses. Both four noded (S4R in ABAQUS) and eight noded (S8R), six degrees of freedom per node, elements were used. Using previous convergence studies as a guideline (Viz et al. 1995a and Viz, 1996), the crack tip region was meshed using square elements with a nodal spacing of $0.02L$, where L is the crack length or other relevant dimension. Special crack tip, or singular elements are not used. The computations were geometrically nonlinear, but materially linear.

To minimize the transverse shear stiffness of the elements, and hence simulate the von-Karman theory, the shell thickness, h , was taken to be small. The finite element model for the problem of a semi-infinite crack in an infinite strip is shown in Figure 4. The model dimensions are $L = 1$, $h = 0.001$, and a length of 20. Symmetry (or anti-symmetry) about $y = 0$ is used to reduce the problem size and to simplify the modeling. The boundary conditions and mesh are given in Figure 4. A simple rectangular mesh of four noded elements is used throughout. A refined mesh of 20×10 elements, each of length $0.02L$ is used in the region surrounding the crack tip.

The finite element model (FEM) for the problem of a small crack in a circular plate is shown in Figure 5. For the analytical approximation given in Section 3.4 to be valid, the crack must be small compared with typical dimensions. Thus the dimensions are $R = 1$, $a = 0.1$ and $h = 0.01$. Past experience shows that $R/a = 10$ is sufficient to approximate a finite crack in an infinite plate. Quarter symmetry is used along $x = 0$ and $y = 0$ to reduce the problem size. Eight node elements are used, and as in the case of infinite strip, the crack tip mesh consists of square elements with a nodal spacing of $0.02a$, element length of $0.04a$.

Let (f_x^n, f_y^n, f_z^n) be the forces, $(M_{xx}^n, M_{yy}^n, M_{zz}^n)$, the moments, (u_x^n, u_y^n, u_z^n) the displacements, and $(\phi_x^n, \phi_y^n, \phi_z^n)$ the rotations at node 'n'. For four node elements, the components of the energy release rate are then given by (Viz et al. 1995a)

$$\begin{aligned}
 G_I &= \frac{f_y^i \Delta u_y^{i-1} + M_{zz}^i \Delta \phi_z^{i-1}}{2h \Delta a}, & G_{II} &= \frac{f_x^i \Delta u_x^{i-1}}{2h \Delta a}, \\
 g_1 &= \frac{M_{xx}^i \Delta \phi_x^{i-1}}{2h \Delta a}, & g_2 &= \frac{f_z^i \Delta u_z^{i-1} + M_{yy}^i \Delta \phi_y^{i-1}}{2h \Delta a},
 \end{aligned} \tag{8a}$$

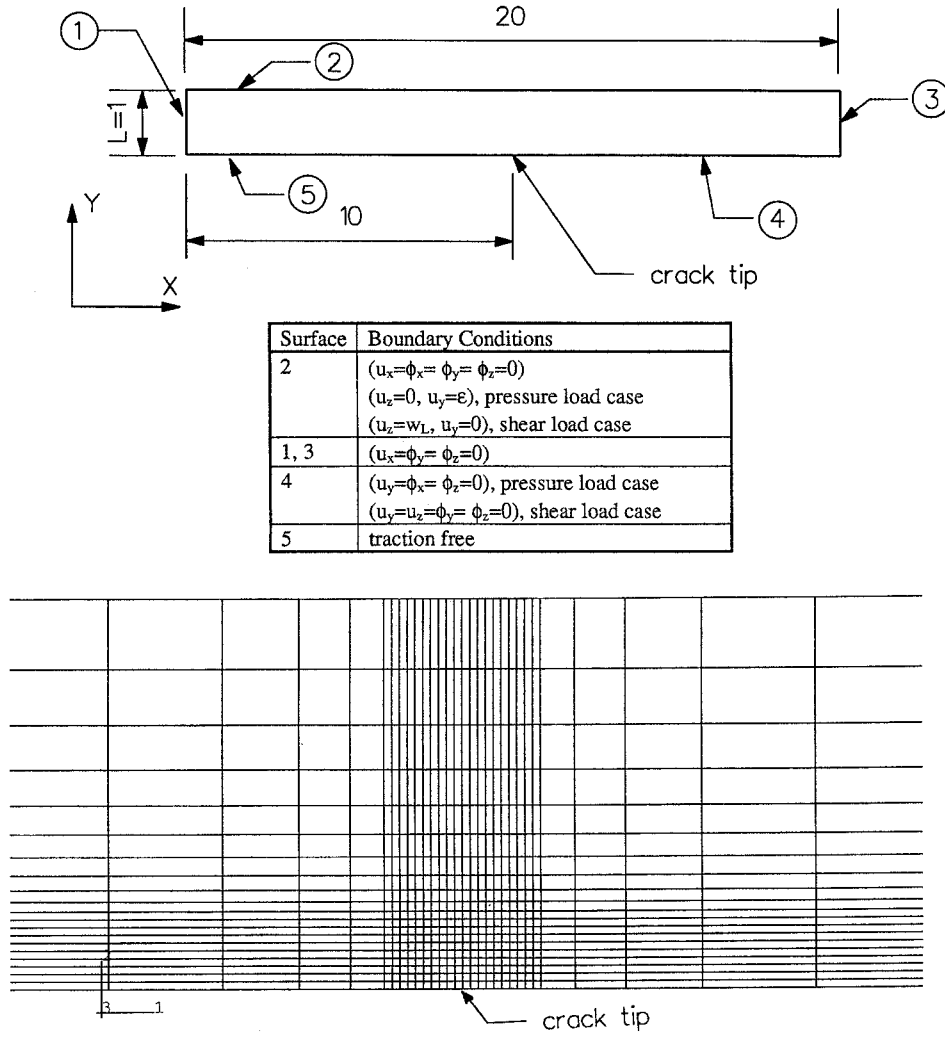


Figure 4. Half plate finite element model used for strip problems (not to scale) and crack tip mesh.

where Δa is the crack tip element length, the \mathbf{f}^i and \mathbf{M}^i are the nodal forces and moments at the crack tip, and $\Delta \mathbf{u}^{i-1}$, $\Delta \phi^{i-1}$ are the jumps across the crack faces in displacements and rotations one node behind the crack tip. For eight node elements the computation is similar

$$\begin{aligned}
 G_I &= \frac{f_y^i \Delta u_y^{i-2} + f_y^{i+1} \Delta u_y^{i-1} + M_{zz}^i \Delta \phi_z^{i-2} + M_{zz}^{i+1} \Delta \phi_z^{i-1}}{2h \Delta a}, \\
 G_{II} &= \frac{f_x^i \Delta u_x^{i-2} + f_x^{i+1} \Delta u_x^{i-1}}{2h \Delta a}, \\
 g_1 &= \frac{M_{xx}^i \Delta \phi_x^{i-2} + M_{xx}^{i+1} \Delta \phi_x^{i-1}}{2h \Delta a}, \\
 g_2 &= \frac{f_z^i \Delta u_z^{i-2} + f_z^{i+1} \Delta u_z^{i-1} + M_{yy}^i \Delta \phi_y^{i-2} + M_{yy}^{i+1} \Delta \phi_y^{i-1}}{2h \Delta a},
 \end{aligned} \tag{8b}$$

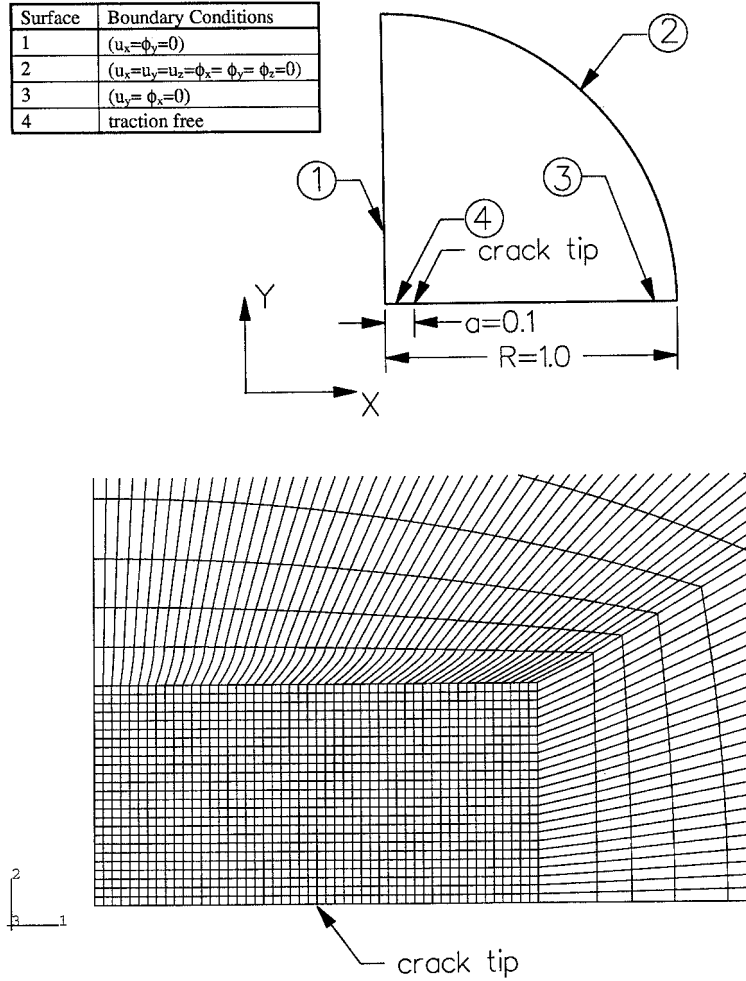


Figure 5. Quarter-plate finite element model used for circular plate problem.

where i is the crack tip node, $i + 1$ is one node ahead of the crack, $i - 1$ is one node behind the crack, and $i - 2$ is two nodes behind the crack. In the G_I calculation, the $M_{zz} \Delta \phi_z$ term is negligible while the $f_z \Delta u_z$ and $M_{yy} \Delta \phi_y$ terms are of equal magnitude in the g_2 calculation. To verify the accuracy of the numerical computations, linear analyses were performed of each case and the computed value of G compared to exact analytical solutions. In all cases the numerical results differed from the exact results by less than 1.5 percent.

3.2. INFINITE STRIP UNDER PRESSURE AND IN-PLANE STRETCHING (ENERGY METHOD)

3.2.1. Problem formulation

The procedure to calculate the energy release rate for the infinite strip problems illustrated in Figure 3 is outlined here. The total energy release rate is calculated based on the definition of G , i.e.

$$G = -\frac{\partial \Pi}{\partial a},$$

where Π is the potential energy of the strip and a is the crack length. Note that as $x \rightarrow \pm\infty$, the stresses and deformation in the strip are independent of x . Now, consider two infinite strips, identical to that shown in Figure 3 but with *no* crack, subjected to the aforementioned stress and deformation states at $x = \pm\infty$. Let $\text{PE}(\pm\infty)$ denote the potential energy per unit length of these strips respectively. Translation invariance in the x direction implies that

$$G = \text{PE}(\infty) - \text{PE}(-\infty). \quad (9)$$

Since N is constant as $x \rightarrow \infty$, $\text{PE}(\infty)$ is

$$\text{PE}(\infty) = \frac{1}{2} \int_{-L}^L N \left[u_y' + \frac{(w')^2}{2} \right] dy + \frac{D}{2} \int_{-L}^L (w'')^2 dy - \int_{-L}^L p w dy. \quad (10a)$$

The first term in the integral is the strain energy associated with the membrane stress, the second term is the strain energy of bending, and the third term represents the external work. Far behind the crack, $x \rightarrow -\infty$, $N = 0$; thus the problem of determining the relation between p and w reverts to a linear one and

$$\text{PE}(-\infty) = -\frac{1}{2} \int_{-L}^L p w dy. \quad (10b)$$

To determine the plate deflection, w as $x \rightarrow \infty$, we note that the only nonvanishing membrane force as $x \rightarrow \infty$ is $N_{22} \equiv N$. Therefore, (3a) reduces to

$$w'''' - (N/D)w'' = p/D, \quad (11)$$

as $x \rightarrow \infty$, where the $' \equiv d/dy$ and p is the external pressure. The unknown membrane force N is determined by integrating the strain stress relation,

$$\varepsilon_{yy} = u_y' + \frac{(w')^2}{2} = \frac{(1-\nu^2)N}{Eh}, \quad (12)$$

from $y = -L$ to L .

The boundary conditions are $w(\pm L) = w'(\pm L) = 0$, and $u_y(\pm L) = \pm\varepsilon L$, (the prestrain). The plate deflection as $x \rightarrow \infty$ is obtained by solving (11) with $p = \text{constant}$,

$$\hat{w} = \frac{12(1-\nu^2)P}{\alpha^3} \left[\frac{\cosh \alpha \eta - \cosh \alpha}{\sinh \alpha} + \frac{1}{2}\alpha(1-\eta^2) \right], \quad (13)$$

where the following normalisations are used

$$\alpha = L\sqrt{N/D}, \quad \eta = y/L, \quad \hat{w} = w/h, \quad P = pL^4/(Eh^4). \quad (14)$$

Integration of (11) using $u_y(\pm L) = \pm\varepsilon L$, yields an equation for the normalized membrane force α as a function of P ,

$$2(\alpha/\delta)^2 \varepsilon + [12(1-\nu^2)P]^2 \Psi_1(\alpha) - \alpha^4/6 = 0, \quad (15a)$$

where $\delta = h/L$, ε is the prestrain and

$$\Psi_1(\alpha) = \alpha^{-2} \left[-\frac{3 \coth \alpha}{2\alpha} + 2\alpha^{-2} + \frac{1}{3} - \frac{\operatorname{cosech}^2 \alpha}{2} \right]. \quad (15b)$$

Given P and ε (15) can be solved for the normalised membrane force α . Once α is known, the energy release rate is found by substituting (13) into (10a) to obtain $PE(\infty)$. Then, using (10a,b) in (9) gives

$$\hat{G} \equiv \frac{GL^3}{Eh^4} = (1 - \nu^2)P^2 \left[\frac{3}{5} - 6\Psi_1(\alpha) - 12\Psi_2(\alpha) \right] + \frac{\varepsilon(\alpha/\delta)^2}{12(1 - \nu^2)}, \quad (16a)$$

where $\Psi_2(\alpha)$ is

$$\Psi_2(\alpha) = -\alpha^{-3} \coth \alpha + \alpha^{-4} + \alpha^{-2}/3, \quad (16b)$$

and \hat{G} is the normalised energy release rate.

3.2.2. Solution in the case of no prestrain, $\varepsilon = 0$

Consider the special case where the strip has no prestrain. The behavior of the normalised membrane force α for small and large pressure can be obtained from the asymptotic behavior of $\Psi_1(\alpha)$, i.e.,

$$\Psi_1(\alpha) \approx \begin{cases} 2\alpha^2/945 & \alpha \ll 1, \\ \alpha^{-2}/3 & \alpha \gg 1, \end{cases} \quad (17)$$

resulting in

$$\alpha^2 \cong \frac{4[12(1 - \nu^2)P]^2}{315} \quad \text{or} \quad N \cong \frac{48(1 - \nu^2)p^2L^6}{315Eh^5}, \quad P \ll 1, \quad (18a)$$

$$\alpha \cong (2[12(1 - \nu^2)P]^2)^{1/6} \quad \text{or} \quad N \cong \left[\frac{Eh^5L^2}{6(1 - \nu^2)} \right]^{1/3} p^{2/3}, \quad P \gg 1. \quad (18b)$$

Note that the membrane force is proportional to p^2 and $p^{2/3}$ at low and high loads respectively.

The behavior of the energy release rate at low and high pressures can be obtained using (16) and the following asymptotic behavior of $\Psi_2(\alpha)$:

$$\Psi_2(\alpha) \approx \begin{cases} 1/45 & \alpha \ll 1, \\ \alpha^{-2}/3 & \alpha \gg 1, \end{cases} \quad (19)$$

resulting in

$$\hat{G} = (1 - \nu^2)P^2/3, \quad P \ll 1, \quad (20a)$$

$$\hat{G} = 3(1 - \nu^2)P^2/5, \quad P \gg 1. \quad (20b)$$

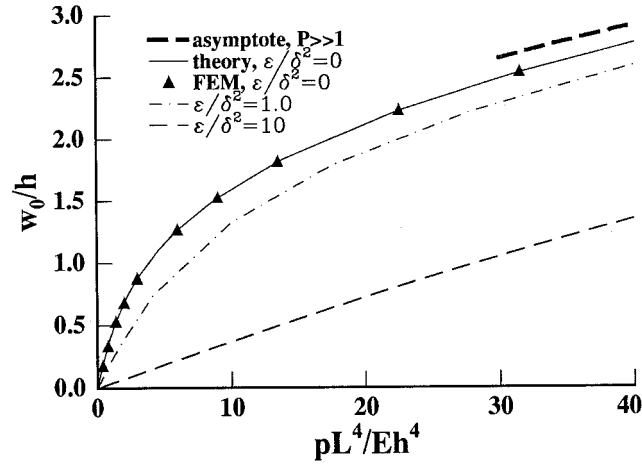


Figure 6. Deflection at the center of strip ($y = 0, x = \infty$) under uniform pressure for various amounts of prestrain.

When the applied pressure is small, we expect that membrane effects can be neglected. The membrane force contribution to the energy release rate is given by the $\Psi_1(\alpha)$ term in (16a), which, at low pressures, according to (17), vanishes as α^2 . The energy of the bending term at $x = \infty$ is given by $\Psi_2(\alpha)$, which is a constant $1/45$ at low pressures. Note also that, a comparison of (20a) and (20b) shows that, at sufficiently high pressures, G is underestimated by the Kirchhoff plate theory by about 44 percent.

The deflection at the middle of the plate ($x \rightarrow \infty, y = 0$), denoted by w_0 , is plotted in Figure 6 as a function of P . From (13), one can show that

$$w_0 \rightarrow \frac{[6(1 - \nu^2)^{1/3} P^{1/3} h]}{2} \quad (21)$$

in the limit $P \gg 1$. This limit is also plotted in Figure 6 which shows that the membrane limit is approached for large plate deflections. The normalised energy release rate \hat{G} versus the normalised pressure P is plotted in Figure 7. The low and high pressure limits given by (20a–b) are also plotted to indicate the range of validity of these asymptotic expressions. This figure shows that over the entire range the energy release rate is approximately proportional to P^2 . The FEM results for \hat{G} are also shown in Figure 7. For $P < 20$, the FEM results agree with the analytical solution to within 2 percent. For $P > 20$, the results begin to diverge slightly since the analytical solution does not take into account very large (elastica like) deflection behind the crack. The close agreement provides confidence in using the finite element program to determine the stress intensity factors, which cannot be obtained in closed form.

In this problem the modes of fracture are the symmetric membrane and bending so that $k_2 = K_{II} = 0$, i.e.,

$$G = G_I + g_1.$$

In the limit of low loads, the contribution of the membrane force to the energy release rate is small compared with those due to bending, so that

$$g_1 \equiv \frac{\pi(1 + \nu)k_1^2}{3(3 + \nu)E} \cong G \cong \frac{Eh^4(1 - \nu^2)P^2}{3L^3}, \quad \text{or} \quad (22a)$$

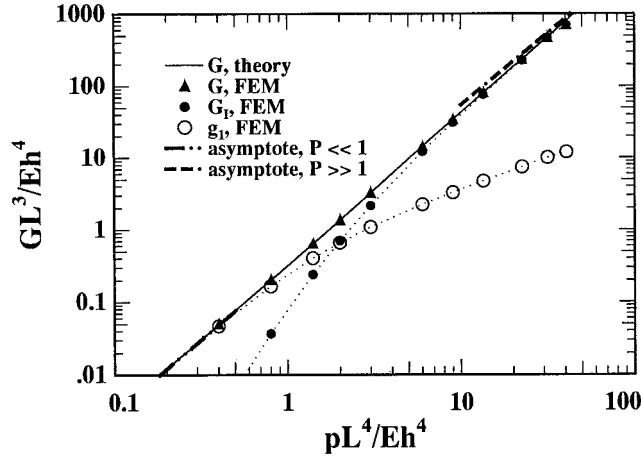


Figure 7. Energy release rate and its components versus pressure for strip under pressure loading, with no prestrain.

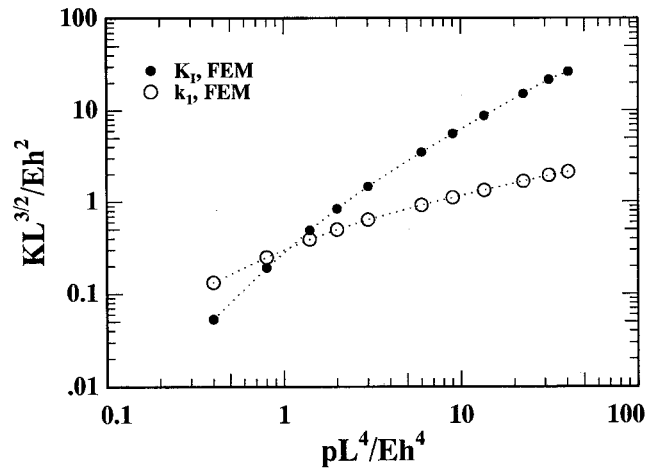


Figure 8. Stress Intensity factors versus pressure for strip under pressure loading with no prestrain.

$$k_I \cong \frac{Eh^2P}{3L^{3/2}} \sqrt{(3+\nu)(1-\nu)/\pi}, \quad K_I/k_I \rightarrow 0, \quad P \ll 1. \quad (22b)$$

Conversely, in the membrane limit, the bending effects are negligible, so that

$$G_I \equiv \frac{K_I^2}{E} \cong G \cong \frac{3Eh^4(1-\nu^2)P^2}{5L^3}, \quad \text{or} \quad (23a)$$

$$K_I \cong \frac{Eh^2P}{L^{3/2}} \sqrt{\frac{3}{5}(1-\nu^2)}, \quad k_I/K_I \rightarrow 0, \quad P \gg 1. \quad (23b)$$

With the exception of these limiting cases, we were unable to find a simple way to decompose G into its components. Thus, FEM was used to determine g_I and G_I and hence k_I , K_I . The FEM results for the energy release rates g_I , G_I , G and stress intensities k_I , K_I are plotted against the normalised pressure P , in Figures 7 and 8 respectively. These figures show that the membrane limit (20a,b) is approached for $P > 5$ corresponding to plate deflection in excess

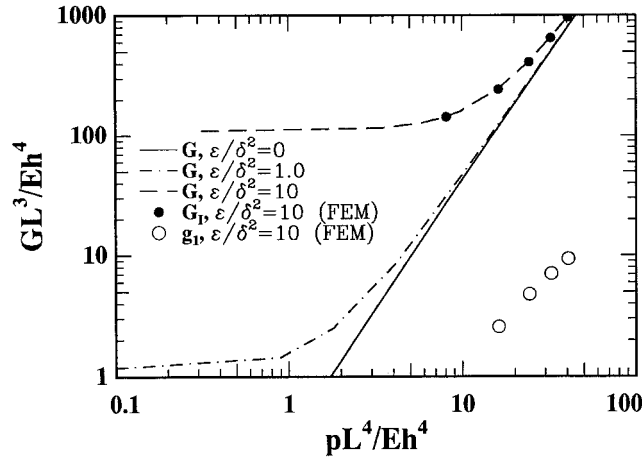


Figure 9. Energy release rate versus pressure for strip under pressure loading, with and without prestrain. Also shown are the energy release rate components for $\varepsilon/\delta^2 = 10$.

of $1.3h$ (see Figure 5). As shown in Figure 7, the bending energy release rate g_1 is significant only for $P < 2$, ($w_0 < 0.7h$).

3.2.3. Solution in the case of prestrain $\varepsilon > 0$

The effect of prestrain is illustrated in Figure 6, which plots w_0/h versus P for $\varepsilon/\delta^2 = 0, 1.0, 10.0$. Equation (15a) shows that the effect of prestrain depends only on the dimensionless parameter $\varepsilon/\delta^2 = L^2\varepsilon/h^2$. For $L/h = 100$, a value of $\varepsilon/\delta^2 = 10$ corresponds to a prestrain of 0.001. Figure 6 shows that even a very small amount of prestrain can significantly affect the transverse stiffness of the plate. This effect is particularly sensitive to the relative plate thickness h/L because of the inverse quadratic dependence.

Figure 9 plots the energy release rates g_1, G_1, G versus the pressure for $\varepsilon/\delta^2 = 10$. The total energy release rate G for $\varepsilon/\delta^2 = 0$ and $\varepsilon/\delta^2 = 1$ are also shown in the same figure. It is clear that, for $\varepsilon/\delta^2 = 10$, the effect of prestrain is that the membrane energy release rate G_1 , completely dominates. The energy release rate G , for small P is given approximately by its plane stress value of

$$G = \frac{EL\varepsilon^2}{(1-\nu^2)}, \quad \text{or} \quad \hat{G} = \frac{GL^3}{Eh^4} = \frac{\varepsilon^2}{\delta^4(1-\nu^2)}. \quad (24)$$

3.3. INFINITE STRIP WITH APPLIED SHEAR DISPLACEMENTS (ENERGY METHOD)

In this problem no pressure loading or prestrain are applied. The plate is loaded by out-of-plane shearing, which induces a combination of K_1 and k_2 fracture modes. We follow the same normalisation of equations and procedure as in 3.2.1. Let the applied shear displacements on the edges $y = \pm L$ be $\pm w_L$ respectively. The boundary conditions are $w(\pm L) = \pm w_L$, $w'(\pm L) = 0$. The plate deflection as $x \rightarrow \infty$, found by solving (11), is

$$\hat{w} = \hat{w}_L \frac{\sinh \alpha \eta - \alpha \eta \cosh \alpha}{\sinh \alpha - \alpha \cosh \alpha}, \quad (25)$$

where $\hat{w}_L = w_L/h$ is the normalised applied displacement. The normalised membrane stress α is determined by integrating (12), to yield

$$6\hat{w}_L^2 \left(1 + \frac{\cosh 2\alpha}{2} - \frac{3 \sinh 2\alpha}{4\alpha} \right) (\sinh \alpha - \alpha \cosh \alpha)^{-2} - 1 = 0. \quad (26)$$

The normalised energy release rate is

$$\hat{G} = \frac{\alpha^4}{144(1-\nu^2)} \left[1 + \left[1 + \frac{\cosh 2\alpha}{2} - \frac{3 \sinh 2\alpha}{4\alpha} \right]^{-1} \left(\frac{\sinh 2\alpha}{2\alpha} - 1 \right) \right]. \quad (27)$$

The behavior of the normalised membrane force α for small and large applied displacements is

$$\alpha^2 \cong 36\hat{w}_L^2/5 \quad \text{or} \quad N \cong \frac{3Ew_L^2h}{[5L^2(1-\nu^2)]}, \quad w_L \ll h, \quad (28a)$$

$$\alpha^2 \cong 6\hat{w}_L^2 \quad \text{or} \quad N \cong \frac{Ew_L^2h}{[4L^2(1-\nu^2)]}, \quad w_L \gg h, \quad (28b)$$

Note that the membrane force is proportional to w_L^2 at both low and high loads.

Using (27) and (28), the energy release rates for small and large applied displacements are

$$\hat{G} \approx \frac{\hat{w}_L^2}{[4(1-\nu^2)]}, \quad w_L \ll h, \quad (29a)$$

$$\hat{G} \approx \frac{\hat{w}_L^4}{[4(1-\nu^2)]}, \quad w_L \gg h, \quad (29b)$$

Figure 10 plots the normalised energy release rate \hat{G} as a function of the normalised displacement \hat{w}_L . The low and high load limits given by (29a,b) are also plotted to indicate the range of validity of these asymptotic expressions. The FEM results for the total energy release rate agree with the analytic solution to within 2 percent.

Symmetry implies that $k_1 = K_{II} = 0$. In the limit of low loads, the membrane effects are negligible, so that by (29a),

$$g_2 \equiv \frac{\pi(1+\nu)k_2^2}{3(3+\nu)E} \cong G \cong \frac{Eh^4\hat{w}_L^2}{4L^3(1-\nu^2)}, \quad \text{and} \quad (30a)$$

$$k_2 \cong \frac{Eh^2\hat{w}_L}{L^{3/2}} \sqrt{\frac{3(3+\nu)}{4\pi(1-\nu^2)(1+\nu)}}, \quad w_L \ll h. \quad (30b)$$

In the membrane limit, the bending effects are negligible, so that by (29b),

$$G_1 \equiv \frac{K_I^2}{E} \cong G \cong \frac{Eh^4\hat{w}_L^4}{4(1-\nu^2)L^3}, \quad (31a)$$

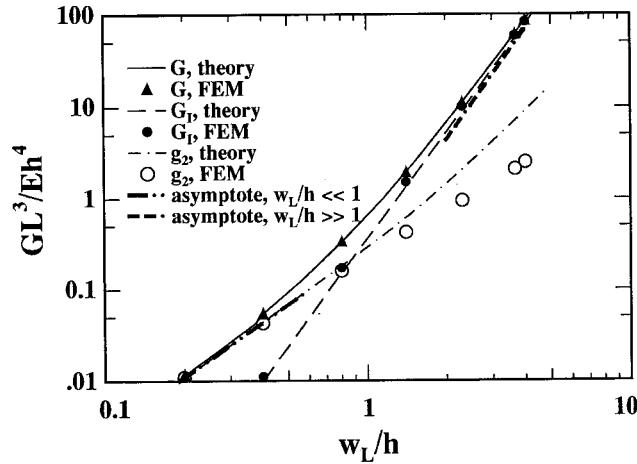


Figure 10. Energy release rate and its components versus out of plane edge shearing deflection for strip under shear loading.

$$K_I \cong \frac{Eh^2 \hat{w}_L^2}{2L^{3/2} \sqrt{1-\nu^2}}, \quad w_L \gg h. \quad (31b)$$

At intermediate displacements, to determine the individual stress intensity factors the energy release rate must be decomposed into tension and bending parts. We propose the following mode decomposition

$$g_2 = \frac{\pi(1+\nu)k_2^2}{3(3+\nu)E} = \frac{D}{2} \int_{-L}^L (w'')^2 dy, \quad (32a)$$

$$G_1 = \frac{K_I^2}{E} = \frac{N}{4} \int_{-L}^L (w')^2 dy, \quad (32b)$$

i.e., g_2 is associated with the strain energy of bending and G_1 with the strain energy of tension. In normalised form, the results are

$$\hat{g}_2 = \frac{\alpha^4}{144(1-\nu^2)} \left[1 + \frac{\cosh 2\alpha}{2} - \frac{3 \sinh 2\alpha}{4\alpha} \right]^{-1} \left(\frac{\sinh 2\alpha}{2\alpha} - 1 \right), \quad (33a)$$

$$\hat{G}_1 = \frac{\alpha^4}{144(1-\nu^2)}. \quad (33b)$$

The stress intensity factors corresponding to this decomposition are

$$\frac{k_2 L^{3/2}}{Eh^2} \cong \sqrt{\frac{3(3+\nu)}{\pi(1+\nu)}} \sqrt{\hat{g}_2}, \quad (34a)$$

$$\frac{K_I L^{3/2}}{Eh^2} \cong \sqrt{\hat{G}_1}. \quad (34b)$$

These mode decomposition results are compared with the FEM calculations in Figures 10 and 11. It is clear that (33) and (34) are not exact, but nevertheless provide an excellent approximation in the entire loading range. The asymptotic results are also plotted on Figure 10. An unexpected result is that extrapolations of the asymptotic results agree extremely well with the finite element results in the *entire loading range*. Therefore, they can replace the more complicated expressions given by (33a,b) and (34a,b). In other words, an excellent approximation for the stress intensity factors is

$$\frac{K_1 L^{3/2}}{Eh^2} \cong \frac{\hat{w}_L^2}{2\sqrt{1-\nu^2}}, \quad \frac{k_2 L^{3/2}}{Eh^2} \cong \frac{E\hat{w}_L}{L^{3/2}} \sqrt{\frac{3(3+\nu)}{4\pi(1-\nu^2)(1+\nu)}}. \quad (35)$$

3.4. CLAMPED CIRCULAR PLATE WITH PRESSURE LOADING (STRESS BASED SOLUTION)

The third example is that of a small crack of length $2a$ in a clamped circular plate of radius R under uniform pressure p . The approach here is simple. We first compute the membrane stress N and the bending moment M , *at the center of the uncracked plate*. The stress intensity factors are then computed by assuming that the crack is in an infinite plate which is subjected to a uniform far-field tension N and bending moment M . In such a situation (Sih et al. 1962)

$$K_1 = N\sqrt{\pi a}/h, \quad k_1 = 6M\sqrt{a}/h^2. \quad (36)$$

Clearly this approach is only valid if $a \ll R$. Otherwise the stress field in the region away from the crack will differ substantially from that of an uncracked plate.

Although there is a closed form solution for the uniformly loaded, uncracked clamped circular plate problem (Conway, 1957; Way, 1934), the results come out as complex expressions. To show very clearly the scalings of the mode couplings, a simple expression for N and M is desired. This is provided by the Foepfel interpolation approach (Conway, 1946; Foepfel and Foepfel, 1924) which assumes ‘that the pressure is composed of two parts, p_1 and p_2 , p_1 causing pure bending and p_2 pure stretching’. For pure bending,

$$\frac{w_0}{h} = \frac{3(1-\nu^2)p_1 R^4}{16Eh^4}, \quad (37a)$$

where w_0 is the deflection at the plate center. Hence the normalised P_1 is

$$P_1 = \frac{p_1 R^4}{Eh^4} = \frac{16w_0}{3(1-\nu^2)h}. \quad (37b)$$

For pure stretching, we find the stress by considering a membrane. For a uniformly loaded membrane, dimensional consideration shows that

$$\frac{w_0}{h} = \beta(\nu) \left(\frac{p_2 R^4}{Eh^4} \right)^{1/3}, \quad (38a)$$

where $\beta(\nu)$ is a dimensionless factor which must be determined by numerical or asymptotic analysis. An FEM analysis employing 10 axisymmetric quadratic shell elements (SAX2 in ABAQUS) was used to compute $\beta(\nu)$. Although these elements have bending and transverse

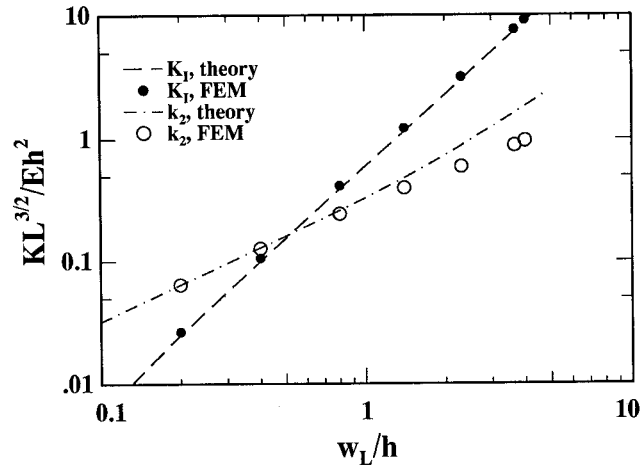


Figure 11. Stress Intensity factors versus out of plane shearing deflection for strip under shear loading.

shear stiffness, these were made negligible by setting $h/R = 10^{-4}$, and by examining the limiting case of large deflections where bending effects are negligible. By simply fitting the results, we find $\beta(\nu = 0.3) = 0.6407$, thus

$$P_2 = \frac{p_2 R^4}{Eh^4} = \left(\frac{w_0}{0.6407h} \right)^3, \quad \nu = 0.3 \quad \text{and} \quad (38b)$$

$$P = P_1 + P_2 = \frac{16w_0}{3(1-\nu^2)h} + \left(\frac{w_0}{0.6407h} \right)^3. \quad (39)$$

A comparison of the prediction of (39), which is based on Foepfel's interpolation method with the exact solution [24] shows excellent agreement. Thus, given the pressure, we can find w_0 by solving (39). The pressures P_1, P_2 can be computed using (37b) and (38b).

In the pure bending problem, the bending moment M at the plate center is

$$\frac{M}{Eh^2} = P_1 \left(\frac{h}{R} \right)^2 \frac{1+\nu}{16}. \quad (40)$$

For the membrane problem, using the known scaling that $N \propto P^{2/3}$, we write

$$\frac{NR^2}{Eh^3} = \gamma(\nu) P_2^{2/3}. \quad (41a)$$

Again by fitting to the axisymmetric FEM results it is found that

$$\frac{NR^2}{Eh^3} = 0.4164 P_2^{2/3}, \quad \nu = 0.3. \quad (41b)$$

The coefficients for the membrane deflection and stress in (38b) and (41b) are within a few percent of the values calculated by Hencky [27] using the finite difference method. The stress intensity factors can be estimated using (40), (41) and (36) and are found to be

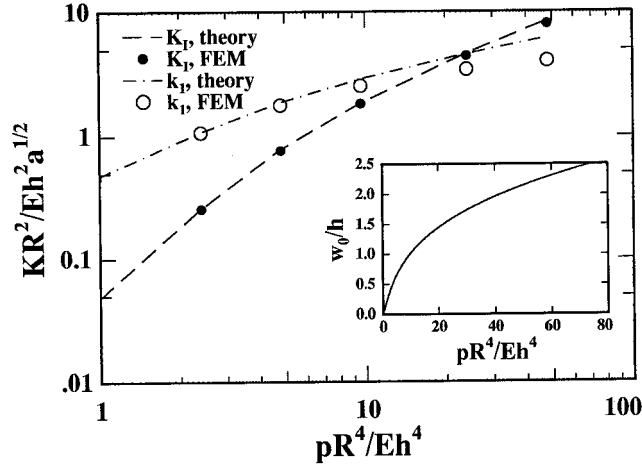


Figure 12. Stress Intensity factors for cracked, clamped circular plate under uniform pressure. The maximum deflection versus pressure for an *uncracked* plate is given in the inset for reference.

$$\frac{R^2 K_1}{Eh^2 \sqrt{a}} = 0.4164 \sqrt{\pi} P_2^{2/3}, \quad \nu = 0.3, \quad (42a)$$

$$\frac{R^2 k_1}{Eh^2 \sqrt{a}} = \frac{6(1 + \nu) P_1}{16}. \quad (42b)$$

The stress intensity factors are plotted versus pressure in Figure 12. Also shown, to help provide a physical interpretation of the pressure values, is the center point deflection of an uncracked plate. The FEM and analytical approximation results agree well up to a normalized pressure of 10. For $P > 10$, the theory predicts K_1 well but underpredicts k_1 . This is similar to the strip under shear loading, where the theory underpredicts k_2 .

4. Discussion and conclusions

Our results show that the stress and deformation field near the crack tip is still comprised of a linear superposition of membrane behavior governed by the plane stress crack tip field and bending behavior governed by the Kirchhoff plate theory crack tip field. An implicit assumption is that the crack length must be substantially larger than the plate thickness and smaller than the in-plane dimensions so that these crack tip fields have a nonzero region of dominance.

The finite element calculations are based on a geometrically nonlinear shell model. The excellent agreements between the total energy release rate calculated using the finite element results and the von Karman theory show that the von Karman theory is a good analytical model for theoretical studies of plate fracture, as long as the deflections are on the order of no more than several plate thicknesses. As expected, our results show that mode coupling becomes important when the plate deflections are on the order of $h/2$ and there is no prestrain. The prestrain has a pronounced effect on the energy release rates. In our example, for a thin enough plate, the bending energy release rate is practically negligible even for a small amount of prestrain. The measure of prestrain is governed by the dimensionless parameter $\varepsilon/\delta^2 = L^2 \varepsilon/h^2$ which is very sensitive to the plate thickness.

Epilogue

Surely Williams met von Karman many times in the halls of Caltech's Guggenheim Aeronautical Laboratories. Perhaps results such as presented here were discussed, perhaps they were too obvious to them to warrant publication. But for us, it is gratifying to know that ad-hoc assumptions made about the crack tip fields in large deflections are, in fact, correct, and hence that current approaches to practical problems in the fracture of plates have a sound theoretical basis.

Acknowledgements

The computations were carried out using the Multi-User Computational Facility of the Cornell Center for Materials Research, supported by NSF, DMR-9632275. The authors thank HKS Corporation for the use of ABAQUS under an academic license. The authors thank Professor H.D. Conway for bringing the Foeppel method to their attention.

References

- Alwar, R.S. and Thiagarajan, S. (1989). Combined effect of shear and large deformation on stress intensity factors. *International Journal of Numerical Methods in Engineering* **28**, 1951–1964.
- Boduroglu, H. and Erdogan, F. (1983). Internal and edge cracks in a plate of finite width under bending. *Journal of Applied Mechanics* **50**, 621–629.
- Conway, H.D. (1946). Large deflection of circular and square plates. *Philosophical Magazine Series 7* **37**, 757–767.
- Conway, H.D. (1957). Notes on Way's large deflection solution for the uniformly loaded and clamped circular plate. *Journal of Applied Mechanics* **24**, 151–152.
- Delale, F. and Erdogan, F. (1979). The effect of transverse shear in a crack plate under skew-symmetric loading. *Journal of Applied Mechanics* **46**, 618–624.
- Foeppel, A. and Foeppel, L. (1924). *Drang und Zwang* **1**, 345.
- Fung, Y.C. (1965). *Fundations of Solid Mechanics*, Prentice-Hall, Englewood Cliffs, New Jersey.
- Hencky, H. (1915). *Z. Math. Physik* **63**, 311.
- Hui, C.Y. and Zehnder, A.T. (1993). A theory for the fracture of thin plates subjected to bending and twisting moments. *International Journal of Fracture* **61**, 211–229.
- Karman, von (1910). T. Festigkeitsprobleme in Maschinenbau. *Encyklopadie der mathematischen Wissenschaften* **IV**, Chap. 27.
- Kirchhoff, G. (1850). Uber das gleichgewicht and die bewegung einer elastischen scheinbe. *J. fuer Reine und Angewandte Mathematik* **40**, 51–88.
- Knowles, J.K. and Wang, N.W. (1960). On the bending of an elastic plate containing a crack. *Journal of Mathematics and Physics* **39**, 223–236.
- Murakami, Y. (1987). *Stress Intensity Factor Handbook* **2**, Pergamon Press, Elmford, New York.
- Murthy, M.V.V., Raju, K.N. and Viswanath, S. (1981). On the bending stress distribution at the tip of a stationary crack from Reissner's theory. *International Journal of Fracture* **17**, 537–552.
- Reissner, E. (1947). On the bending of elastic plates. *Quarterly of Applied Mathematics* **5**, 55–68.
- Sih, G.C., Paris, P.C. and Erdogan, F. (1962). Crack tip stress intensity factors for plane extension and plate bending problems. *Journal of Applied Mechanics* **29**, 306–312.
- Simmonds, J.G. and Duva, J. (1981). Thickness effects are minor in the energy release rate integral for bent plates containing elliptical holes or cracks. *Journal of Applied Mechanics* **48**, 320–326.
- Viz, M.J. (1996). *Fatigue Fracture of 2024-T3 Aluminum Plates under In-plane Symmetric and out of Plane Anti-symmetric Mixed-mode Deformations*, Ph.D thesis, Cornell University.
- Viz, M.J. and Zehnder, A.T. (1994). *Fatigue Crack Growth in 2024-T3 Aluminum under Tensile and Transverse Shear Stresses*, in FAA/NASA International symposium on advanced structural integrity methods for airframe durability and damage tolerance, NASA CP-3274, C. Harris, eds, 891–910.

- Viz, M.J., Potyondy, D.O., Zehnder, A.T., Rankin, C.C. and Riks, E. (1995a). Computation of membrane and bending stress intensity factors for thin cracked plates. *International Journal of Fracture* **72**, 21–38.
- Viz, M.J., Zehnder, A.T. and Bamford, J.D. (1995b). Fatigue fracture of thin plates under tensile and transverse shear stresses, in *Fracture Mechanics* **26**, ASTM STP 1256. Reuter et al, eds, American Society for Testing and Materials, Philadelphia, PA, 631–651.
- Wang, N.M. (1970). Twisting of an elastic plate containing a crack. *International Journal of Fracture Mechanics* **6**, 367–378.
- Way, S. (1934). Bending of circular plates with large deflections. *Transactions ASME* **56**, 627.
- Williams, M.L. (1961). The bending stress distribution at the base of a stationary crack. *Journal of Applied Mechanics* **28**, 78–82.
- Young, M.J. and Sun, C.T. (1993a). Crack plates subjected to out of plane tearing loads. *International Journal of Fracture* **60**, 1–18.
- Young, M.J. and Sun, C.T. (1993b). On the strain energy release rate for crack plate subjected to out of plane bending moment. *International Journal of Fracture* **60**, 227–247.
- Zehnder, A.T. and Hui, C.Y. (1994). Stress Intensity Factors for Plate Bending and Shearing problems. *Journal of Applied Mechanics* **61**, 719–722.